Photoluminescence Properties of Pr-Doped (Ca,Sr,Ba)TiO_3

Tôru Kyômen, Riichiro Sakamoto, Norihiko Sakamoto, Syunsuke Kunugi, and Mitsuru Itoh*

Materials and Structures Laboratory, Tokyo Institute of Technology, 4259 Nagatsuta, Midori-ku, Yokohama 226-8503, Japan

Received September 15, 2004. Revised Manuscript Received February 17, 2005

Photoluminescence properties of Pr-doped alkaline-earth titanates $Pr_{0.002}(Ca,Sr,Ba)_{0.997}TiO_3$ are investigated by emission, excitation, and diffuse reflectance spectra at room temperature. The intensities of red luminescence and absorption due to $f-f$ transition of Pr^{3+} ions increase in the order of Pr-doped cubic $SrTiO_3$, tetragonal $BaTiO_3$, and orthorhombic $CaTiO_3$. The small red luminescence for Pr-doped $SrTiO_3$ is increased by substituting Sr by Ca and Ba even if the substituted samples have the same cubic structure as $SrTiO_3$ and the lattice parameters are close to that of $SrTiO_3$. The red luminescence intensity is intense for orthorhombic samples of which the excitation spectra show a peak corresponding to valence-to-conduction band edge and a shoulder referred to as B band. The photoluminescence properties are discussed in relation to the crystal structure.

Introduction

Rare-earth ions are often used as activators for light-emitting materials. The light emission usually originates from $4f^n-4f^n$ transition via excited states such as charge transfer (CT) state between rare-earth ions and ligand ions, $4f^{n-1}5d^1$ state of rare-earth ions, and so on. Because factors to determine the light-emitting properties such as $4f^n-4f^n$ transition probability and relaxation process from the excited state to $4f^n$ excited state are affected by host materials, it is important to understand the relation between the factors and environment of rare-earth ions in solids. Recently, luminescence properties of Pr-doped alkaline-earth titanates with a perovskite-type structure have been investigated because of the strong red emission as summarized in the next paragraph. The perovskite-type oxides, ABO_3, are materials of which the physical properties, such as electric, magnetic, dielectric properties, and so on, have been widely investigated in relation to the crystal structure because the materials have relatively simple but various crystal structures that can be changed by substitutions of both A and B site ions with large fraction. Therefore, Pr-doped alkaline-earth titanates are suitable materials for the investigation of the relationship between light-emitting properties and crystal structure.

Diallo et al. first reported that Pr-doped $CaTiO_3$ shows intense red emission by ultraviolet (UV) light excitation.[1,2] The red emission is ascribed to $4f^2-4f^2$ transition of Pr^{3+} ions from the excited state $^1D_2$ to the ground state $^3H_4$. In addition, they observed a shoulder (referred to as B band) in the low-energy side of the valence-to-conduction band (referred to as A band) edge in the diffuse reflectance spectrum of Pr-doped $CaTiO_3$ and ascribed it to the $4f^15d^1$ band of Pr^{3+} ions. Based on these results, they proposed that an energy transfer occurs to the excited 4f or 5d levels of Pr^{3+} ions after valence-to-conduction band transition, in other words, CT transition from oxygen to titanium ions, by UV light excitation. Recently, Boutinaud et al. proposed that the B band is ascribed to Pr^{3+}/Ti^{4+}-to-Pr^{4+}/Ti^{3+} CT transition.[3] Although the red luminescence intensity of Pr-doped $SrTiO_3$ is very small, Okamoto et al. reported that Pr-doped $SrTiO_3$ synthesized with 23 mol % Al shows a strong red photoluminescence about 200 times higher than that for Al-free samples.[4] At the same time, Itoh et al. reported that Pr-doped $SrTiO_3$ with addition of Al shows a strong red emission by low-voltage electron excitation.[5] Since these reports, the substitution of Ti^{4+} ions in $SrTiO_3$ and $BaTiO_3$ by trivalent ions such as Al^{3+}, Ga^{3+}, and In^{3+} have been reported to enhance the red luminescence intensity.[6−10] Jia et al. reported that the red luminescence intensity of Pr-doped $Sr_{1-x}Ca_xTiO_3$ increases with increasing x and suggested that an energy transfer from Pr ions to the CT state of TiO_6^{8-} complex is a reason for the small red emission intensity of Pr-doped $SrTiO_3$.[11]

The A and B band edges are expected to be controlled to some extent by mixing Ca, Sr, and Ba ions at the alkaline-earth site. In the present study, photoluminescence properties are investigated for Pr-doped (Ca,Sr,Ba)TiO_3 solid-solution materials. The photoluminescence properties are discussed in relation to the solid-solution effect at the alkaline-earth site and the average radius of the alkaline-earth ions.

* To whom correspondence should be addressed.

(1) Diallo, P. T.; Boutinaud, P.; Mahiou, R.; Cousseins, J. C. *Phys. Status Solidi A* **1997**, *160*, 255.
(2) Diallo, P. T.; Jeanlouis, K.; Boutinaud, P.; Mahiou, R.; Cousseins, J. C. *J. Alloys Compd.* **2001**, *323−324*, 218.
(3) Boutinaud, P.; Pinel, E.; Dubois, M.; Vink, A. P.; Mahiou, R. *J. Luminescence* **2005**, *111*, 69.
(4) Okamoto, S.; Kobayashi, H.; Yamamoto, H. *J. Appl. Phys.* **1999**, *86*, 5594.
(5) Itoh, S.; Toki, H.; Tamura, K.; Kataoka, F. *Jpn. J. Appl. Phys.* **1999**, *38*, 6387.
(6) Okamoto, S.; Tanaka, S.; Yamamoto, H. *Int. J. Mod. Phys. B* **2001**, *15*, 3924.
(7) Okamoto, S.; Yamamoto, H. *Appl. Phys. Lett.* **2001**, *78*, 655.
(8) An, H.-K.; Kang, S.; Suh, K.-S. *J. Mater. Sci.* **2001**, *12*, 157.
(9) Okamoto, S.; Yamamoto, H. *J. Appl. Phys.* **2002**, *91*, 5492.
(10) Yamamoto, H.; Okamoto, S.; Kobayashi, H. *J. Luminescence* **2002**, *100*, 325.
(11) Jia, W.; Xu, W.; Rivera, I.; Perez, A.; Fernandez, F. *Solid State Commun.* **2003**, *126*, 153.

10.1021/cm0403715 CCC: $30.25
Published on Web 05/12/2005

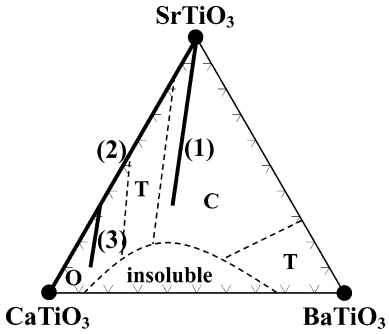

Figure 1. Phase diagram of (Ca,Sr,Ba)TiO$_3$.[13] C (cubic), T (tetragonal), and O (orthorhombic) indicate the crystal system of samples in the respective region. Dots and thick lines indicate compositions of prepared samples.

Table 1. Compositions and Lattice Parameters of Prepared $Pr_z(Ca_{1-x-y}Sr_xBa_y)_{0.997}TiO_3$ on Line (1) in Figure 1; Space Group Is *Pm*3*m*

x	*y*	*z*	*a* (Å)
1	0	0.0024(3)	3.9050(4)
0.7	0.111	0.0023(3)	3.904(1)
0.5	0.185	0.0024(3)	3.902(2)
0.35	0.241	0.0023(3)	3.902(3)

Experimental Section

Pr-doped (Ca,Sr,Ba)TiO$_3$ polycrystalline samples were prepared by a solid-state reaction method. Appropriate amounts of $CaCO_3$, $SrCO_3$, $BaCO_3$, TiO_2, and Pr_6O_{11} corresponding to $Pr_{0.002}(Ca_{1-x-y}Sr_xBa_y)_{0.997}TiO_3$ were mixed in an agate mortar with ethanol and calcined in air at 1273 K. The calcined powder was pressed into pellets and sintered in air at 1623 K for 6 h. The temperature was successively decreased to 1273 K; the sample was annealed there for 12 h and then cooled to room temperature in the furnace. The pellets were ground and the obtained powders were used for measurements. The content of Pr ions at the alkaline-earth site was fixed at 0.2%. The actual Pr contents were determined by inductively coupled plasma (ICP) spectroscopy using a HORIBA Ultima2 instruments. The results are tabulated in Tables 1−3. The samples are named as Pr-doped $Ca_{1-x-y}Sr_xBa_yTiO_3$ in this paper for simplicity.

Powder X-ray diffraction measurements were carried out using Cu Kα radiation (MAC Science, MXP18HF). Lattice parameters were determined from some diffraction peaks in a high 2θ region using Si crystalline powder as an internal standard. Emission and excitation spectra were measured in air at room temperature by using a spectrofluorometer (JASCO, FP-6500). Diffuse reflectance spectra were measured in air at room temperature by using a spectrophotometer (Barian, CARY 500).

The phase diagram of (Ca,Sr,Ba)TiO$_3$ has been reported earlier[13] as shown in Figure 1. In addition to Pr-doped $CaTiO_3$, $SrTiO_3$, and $BaTiO_3$, some solid-solution samples, the compositions of which are located on the thick lines (1), (2), and (3) in the figure, were prepared. We paid attention to the average size of alkaline-earth ions. The compositions of samples on the line (1) are tabulated in Table 1 and obey the equation

$$(1-x-y)r_{Ca} + xr_{Sr} + yr_{Ba} = r_{Sr} \quad (1)$$

where r_A's are Shannon ion radii of A^{2+} ions at the twelve-coordinated site.[14] For these samples, it is expected that the crystal structures are close to that of $SrTiO_3$. In fact, the crystal systems of these samples are cubic and the lattice parameters are close to that of $SrTiO_3$ as shown in Table 1. The compositions of samples on line (2) in Figure 1 are tabulated in Table 2. The XRD peaks of samples were indexed by the space groups reported in the literature.[12] A perovskite parameter defined as $a_p = V^{1/3}$, where V is the volume per ABO_3, is often used instead of the unit cell volume in order to compare the unit cell size of perovskite-type oxides with different unit cells. It is found that the perovskite parameter decreases with decreasing x due to the fact that Ca^{2+} ion is smaller than Sr^{2+} ion. The space group, point symmetry at the alkaline-earth site, and the number of symmetry operations for these samples are shown in Table 2. The compositions of samples on line (3) obey the equation

$$(1-x-y)r_{Ca} + xr_{Sr} + yr_{Ba} = 0.35r_{Sr} + 0.65r_{Ca} \quad (2)$$

The XRD peaks of these samples were indexed by the *Pnma* space group. The compositions and lattice parameters are tabulated in Table 3. It is found that the lattice parameters and the perovskite parameter are nearly the same for these samples.

Table 2. Compositions, Perovskite Parameter (a_p), Space Group (S.G.), Point Symmetry (P.S.) at the Alkaline-Earth Site, and the Number of Symmetry Operations (N.S.O.) of Prepared $Pr_z(Ca_{1-x}Sr_x)_{0.997}TiO_3$ on Line (2) in Figure 1

x	*z*	a_p (Å)	S.G.	P.S.	N.S.O.
1	0.0024(3)	3.905	*Pm*3*m*	O_h	48
0.8	0.0024(3)	3.892	*I*4/*mcm*	D_{2d}	8
0.7	0.0023(3)	3.883	*I*4/*mcm*	D_{2d}	8
0.6	0.0023(3)	3.876	*Bmmb*	C_{2v}	4
0.5	0.0025(3)	3.869	*BmmB*	C_{2v}	4
0.4	0.0023(3)	3.860	*Pnma*	C_{1h}	2
0.35	0.0024(3)	3.855	*Pnma*	C_{1h}	2
0.3	0.0023(3)	3.851	*Pnma*	C_{1h}	2
0	0.0024(3)	3.824	*Pnma*	C_{1h}	2

Table 3. Compositions, Lattice Parameters, and Perovskite Parameter of Prepared $Pr_z(Ca_{1-x-y}Sr_xBa_y)_{0.997}TiO_3$ on Line (3) in Figure 1; Space Group Is *Pnma*

x	*y*	*z*	*a* (Å)	*b* (Å)	*c* (Å)	a_p (Å)
0.35	0	0.0023(3)	5.4581(1)	7.7080(1)	5.4466(1)	3.855
0.2	0.05	0.0022(3)	5.4582(9)	7.7070(7)	5.435(1)	3.852
0.1	0.09	0.0023(3)	5.461(1)	7.704(1)	5.435(1)	3.852

Results

Pr-Doped $CaTiO_3$, $SrTiO_3$, and $BaTiO_3$. Figure 2a shows the excitation spectra monitored at 613 nm (left) and the emission spectra excited by 335 nm light (right) for Pr-doped $CaTiO_3$, $SrTiO_3$, and $BaTiO_3$. The enlarged figure is shown in Figure 3a. Pr-doped $CaTiO_3$ shows intense red emission with a peak at 613 nm, as reported by Diallo et al.[1,2] In contrast, the red luminescence intensities are very weak for Pr-doped $SrTiO_3$ and $BaTiO_3$. The red luminescence intensity increases in the order of Pr-doped $SrTiO_3$, $BaTiO_3$, and $CaTiO_3$, as found from Figure 3a. The intensity of the peak at 613 nm in the emission spectrum of Pr-doped $CaTiO_3$ is about 200 times larger than that of Pr-doped $BaTiO_3$. The excitation spectrum of Pr-doped $CaTiO_3$ shows a peak at 335 nm and a shoulder around 380 nm as reported by Diallo et al.[1,2]

Figure 2b shows the diffuse reflectance spectra for Pr-doped $CaTiO_3$, $SrTiO_3$, and $BaTiO_3$. The enlarged figure is shown in Figure 3b. The valence-to-conduction band edges are observed around 335, 365, and 370 nm respectively for Pr-doped $CaTiO_3$, $SrTiO_3$, and $BaTiO_3$. In addition, a

(12) Ball, C. J.; Begg, B. D.; Cookson, D. J.; Thorogood, G. J.; Vance, E. R. *J. Solid State Chem.* **1998**, *139*, 238.
(13) McQuarrie, M. *J. Am. Ceram. Soc.* **1955**, *38*, 444.
(14) Shannon, R. D. *Acta Crystallgr. A* **1976**, *32*, 751.

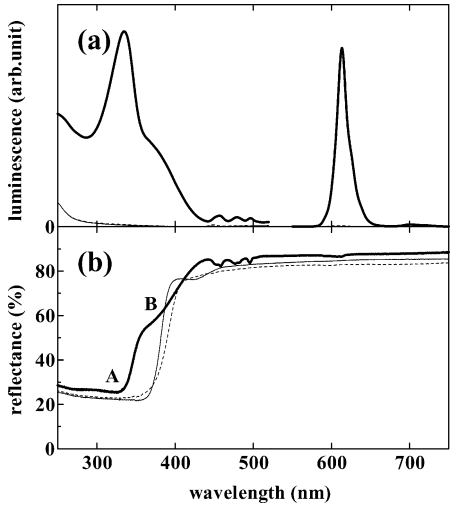

Figure 2. (a) Excitation spectra monitored at 613 nm (left) and emission spectra excited by 335 nm light (right) and (b) diffuse reflectance spectra: Thick lines, $Pr_{0.002}Ca_{0.997}TiO_3$; thin lines, $Pr_{0.002}Sr_{0.997}TiO_3$; dashed lines, $Pr_{0.002}Ba_{0.997}TiO_3$.

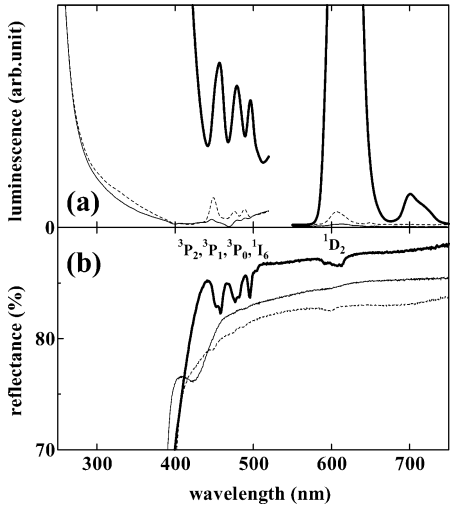

Figure 3. (a) Excitation spectra monitored at 613 nm (left) and emission spectra excited by 335 nm light (right) and (b) diffuse reflectance spectra on an enlarged scale: Thick lines, $Pr_{0.002}Ca_{0.997}TiO_3$; thin lines, $Pr_{0.002}Sr_{0.997}TiO_3$; dashed lines, $Pr_{0.002}Ba_{0.997}TiO_3$.

shoulder is observed in the long-wavelength side of the band edge for Pr-doped $CaTiO_3$ as reported by Diallo et al.[1,2] According to them, the conduction band and the absorption band corresponding to the shoulder are referred to as A and B band, respectively, in this paper. It should be noted that the wavelengths of the valence-to-conduction band edge and B band edge for Pr-doped $CaTiO_3$ are coincident with those of the peak and shoulder observed in the excitation spectrum shown in Figure 2a. The absorption intensities due to f−f transitions of Pr^{3+} ions from $^3H_4$ to ^3P_J, $^1I_6$, and $^1D_2$ are strong for Pr-doped $CaTiO_3$, weak for Pr-doped $BaTiO_3$, and very weak for Pr-doped $SrTiO_3$. Another absorption is observed around 420 nm for Pr-doped $SrTiO_3$, the origin of which is unclear at present.

Pr-Doped Cubic $Ca_{1-x-y}Sr_xBa_yTiO_3$. Figure 4a shows the excitation spectra monitored at 613 nm for the cubic solid-solution samples in Table 1 and the emission spectra excited by light with wavelength at which the excitation spectrum shows a peak. The red luminescence intensity increases with decreasing Sr content. But the peak intensity

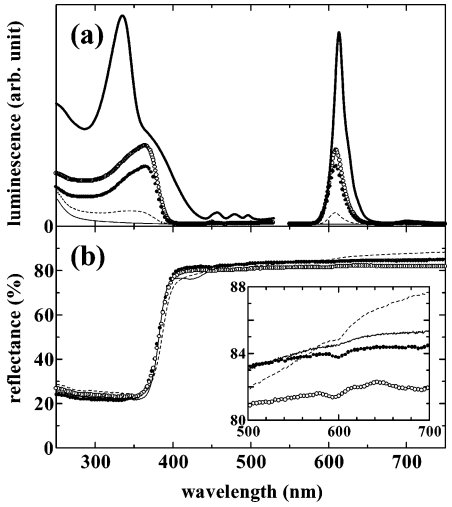

Figure 4. (a) Excitation spectra monitored at 613 nm (left) and emission spectra (right) and (b) diffuse reflectance spectra for cubic $Pr_{0.002}(Ca_{1-x-y}Sr_xBa_y)_{0.997}TiO_3$ in Table 1: Thin lines, $x = 1$; dashed lines, $x = 0.7$; solid circles, $x = 0.5$; open circles, $x = 0.35$. The inset shows the enlarged figure of (b). The excitation and emission spectra for $Pr_{0.002}Ca_{0.997}TiO_3$ are also plotted by thick lines in (a) for comparison.

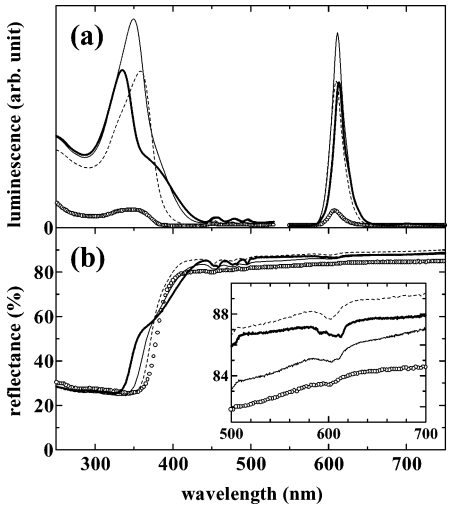

Figure 5. (a) Excitation spectra monitored at 613 nm (left) and emission spectra (right) and (b) diffuse reflectance spectra for $Pr_{0.002}(Ca_{1-x}Sr_x)_{0.997}TiO_3$ in Table 2: Thick solid lines, $x = 0$; thin solid lines, $x = 0.35$; dashed lines, $x = 0.6$; open circles, $x = 0.8$. The inset shows the enlarged figure of (b).

is at most half of that for Pr-doped $CaTiO_3$ indicated by the thick solid lines in the figure. Contrary to the excitation spectrum of Pr-doped $CaTiO_3$, the excitation spectra of these samples show only a peak around 365 nm but no shoulder. Figure 4b shows the diffuse reflectance spectra for these samples. The valence-to-conduction band edges are nearly the same for these samples. It should be noted that the wavelengths of peaks in the excitation spectra are coincident with the band edges. Contrary to the spectrum of Pr-doped $CaTiO_3$, there is no shoulder corresponding to the B band edge. The absorption intensities due to f−f transitions of Pr^{3+} ions are large for the solid-solution samples as compared to that for Pr-doped $SrTiO_3$, as exemplified by the $^3H_4$-to-$^1D_2$ transition shown in the inset of Figure 4b.

Pr-Doped $Ca_{1-x}Sr_xTiO_3$. Figure 5a shows the excitation spectra monitored at 613 nm for some samples in Table 2 and the emission spectra excited by light with wavelength at which the excitation spectrum shows a peak. Figure 5b)

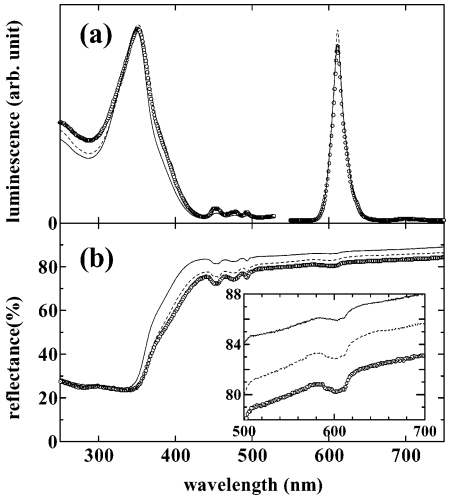

Figure 6. (a) Excitation spectra monitored at 613 nm (left) and emission spectra (right) and (b) diffuse reflectance spectra for orthorhombic $Pr_{0.002}(Ca_{1-x-y}Sr_xBa_y)_{0.997}TiO_3$ in Table 3: Solid lines, $y = 0$; dashed lines, $y = 0.05$; open circles, $y = 0.09$. The inset shows the enlarged figure of (b).

shows the diffuse reflectance spectra of these samples. As x increases, the valence-to-conduction band edge around 335 nm observed for Pr-doped $CaTiO_3$ shifts to the long-wavelength side, and the peak in the excitation spectrum around 335 nm observed for Pr-doped $CaTiO_3$ also shifts to the long-wavelength side. On the other hand, the shoulders around 380 nm observed in the excitation and diffuse reflectance spectra of Pr-doped $CaTiO_3$ shift to the short-wavelength side with increasing x. The absorption intensities due to the $^3H_4$-to-$^1D_2$ transition for the $x = 0$ sample is similar to (or slightly larger than) that of the $x = 0.35$ sample but clearly larger than those for $x = 0.6$ and 0.8 samples, as found from the inset of Figure 5b.

Pr-Doped Orthorhombic $Ca_{1-x-y}Sr_xBa_yTiO_3$. Figure 6a shows the excitation spectra monitored at 613 nm for the orthorhombic solid-solution samples in Table 3 and the emission spectra excited by light with wavelength at which the excitation spectrum shows a peak. The red luminescence intensities are nearly the same for these samples. Figure 6b shows the diffuse reflectance spectra of these samples. The wavelengths of valence-to-conduction band edge around 340 nm and B band edge around 380 nm are also nearly the same for these samples. The absorption intensities due to the $^3H_4$-to-$^1D_2$ transition for the $y = 0.09$ sample seems to be larger than that for the $y = 0$ sample, as found from the inset of Figure 6b.

Discussion

As mentioned in section 1, it is expected that A and B band edges are controlled by mixing Ca, Sr, and Ba ions at the alkaline-earth site. In fact, the valence-to-conduction band edges (A band edges) are nearly the same for the cubic solid-solution samples with the same average radius of alkaline-earth ions. In addition to the A band edges, the B band edges are also the same for the orthorhombic solid-solution samples with the same average radius of alkaline-earth ions. These results suggest that both A and B band edges are determined by the average radius of alkaline-earth ions.

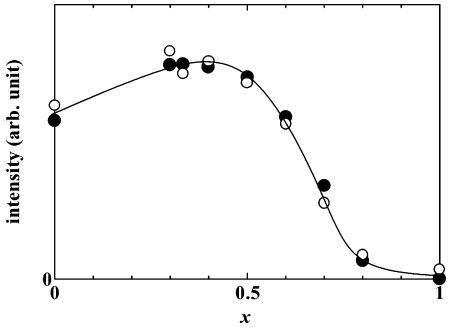

Figure 7. Intensity of red luminescence as a function of x for $Pr_{0.002}(Ca_{1-x}Sr_x)_{0.997}TiO_3$: Solid circles, peak intensity of excitation spectrum; open circles, integral of the excitation spectrum in the range 250−430 nm.

Despite this, the red luminescence intensities of the cubic solid-solution samples are much larger than that of Pr-doped $SrTiO_3$. The reason for this enhancement would be understood as follows. The electric dipole transition between $4f^n$ levels is forbidden when a rare-earth ion is located at a centrosymmetric site. In fact, the absorption intensities of f−f transitions are very small for Pr-doped $SrTiO_3$ because of the centrosymmetric Sr site (O_h) in $SrTiO_3$. In contrast, the absorption intensities are large for Pr-doped $BaTiO_3$ and $CaTiO_3$ because of the noncentrosymmetric Ba site (C_{4v}) in $BaTiO_3$ and Ca site (C_{1h}) in $CaTiO_3$. For the cubic solid-solution samples, even if the crystallographic point symmetry at the alkaline-earth site is O_h, the local point symmetry is supposed to be lower than it because of the random occupation at the alkaline-earth site by Ca, Sr, and Ba ions with different ion radii. The f−f transitions would be thus allowed due to the lowered local point symmetry. In fact, the absorption intensities of f−f transitions for the cubic solid-solution samples are much larger than that of Pr-doped $SrTiO_3$, as found from the inset of Figure 4b.

The solid circles in Figure 7 show the intensity of the peaks in the excitation spectra for Pr-doped $Ca_{1-x}Sr_xTiO_3$. The open circles in the figure show the integrals of the excitation spectra in the range 250−430 nm. Both the intensities show similar behaviors; first, the intensities drastically decrease above about $x = 0.5$ and second the intensities decrease with decreasing x below about $x = 0.4$. The first behavior is understood by the f−f transition probability decreased with increasing x because the absorption intensities due to the $f - f$ transitions for $x = 0.6$ and 0.8 samples are smaller than that for the $x = 0.35$ sample. This may be connected with the point symmetry at the alkaline-earth site, judging from the fact that the number of symmetry operations increases with increasing x (these are still noncentrosymmetric sites) as indicated in Table 1. One may consider that the second behavior is also connected with the f−f transition probability because the randomness at the alkaline-earth site should increase from $x = 0$ to $x = 0.4$. However, the absorption intensity of the $x = 0.35$ sample is not larger than that of the $x = 0$ sample, as found from the inset of Figure 5b. Therefore, another reason would be necessary to explain the second behavior. According to Diallo et al.,[1,2] it is expected that there are two processes for the red emission of the Ca-rich samples. One is that the valence-to-conduction band absorption first occurs, the energy of the excited electrons is transferred to Pr ions, and the excited Pr ions emit the red

light. The other is that the excitation to B band (clearly connected with the excited state of Pr ions) first occurs and then the excited Pr ions emit the red light. If two contributions are superposed in the same wavelength region, the peak intensity of red luminescence increases naturally. In fact, A and B band edges shift to the opposite wavelength side with increasing x, as found from Figure 5, and thus the two contributions should be superposed at a certain x. Therefore, the maximum red luminescence intensity around $x = 0.4$ can be understood qualitatively by the superposition of the two contributions.

Conclusions

In the present study, photoluminescence properties of Pr-doped alkaline-earth titanates $Pr_{0.002}(Ca,Sr,Ba)_{0.997}TiO_3$ are investigated at room temperature. For pure host materials, intensities of red luminescence and absorption of f−f transitions of Pr^{3+} ions increase in the order of cubic $SrTiO_3$, tetragonal $BaTiO_3$, and orthorhombic $CaTiO_3$. The small intensities for $SrTiO_3$ increase when the Sr^{2+} ions are substituted by Ca^{2+} and Ba^{2+} ions, even if the average radius of the alkaline-earth ions is the same as that of Sr^{2+} ion. The intense red luminescence is observed for Ca-rich samples with orthorhombic structure. The red luminescence intensity shows a maximum around $x = 0.4$ for Pr-doped $Ca_{1-x}Sr_xTiO_3$. The A and B band edges shift to long- and short-wavelength sides, respectively, with increasing the average radius of alkaline-earth ions.

We propose the following. The f−f transition probability increases due to lowering the point symmetry at the alkaline-earth site which can be controlled by either crystallographic site symmetry or solid-solution effect at the alkaline-earth site. Some luminescence properties such as intensity and peak wavelength in the excitation spectrum can be controlled to some extent by the average radius of alkaline-earth ions.

Acknowledgment. The authors wish to thank Dr. Katsumata and Prof. Inaguma of Gakusyuin University for ICP measurements and useful discussions.

CM0403715